Rydberg and continuum states of the HeH^+ molecular ion: Variational R-matrix and multichannel quantum defect theory calculations

I. Bouhali,[1] S. Bezzaouia,[1] M. Telmini,[1] and Ch. Jungen[2,3]

[1]*LSAMA Department of Physics, Faculty of Science of Tunis, University of Tunis El Manar, 2092 Tunis, Tunisia*

[2]*Laboratoire Aimé Cotton du CNRS, Université de Paris-Sud, F-91405 Orsay, France*

[3]*Department of Physics and Astronomy, University College London, London WC1E 6BT, United Kingdom*

(Received 28 June 2016; published 31 August 2016)

Variational *ab initio* R-matrix theory combined with generalized multichannel quantum defect theory is used to calculate singly excited Rydberg states of the hydrohelium molecular ion, HeH^+, for $^{1,3}\Sigma^+$, $^{1,3}\Pi$, $^{1,3}\Delta$, $^{1,3}\Phi$, and $^{1,3}\Gamma$ symmetry. Bound levels are calculated for n values up to $n \approx 10$, and continuum states up to ≈3 eV above the HeH^{2+} threshold. The calculations span the range of internuclear distances R from 1 to 5 bohrs. The present work follows a preliminary study on the $^{1,3}\Delta$ states of HeH^+ [Bouhali, Bezzaouia, Telmini, and Jungen, EPJ Web Conf. **84**, 04004 (2015)] which was also based on R-matrix theory. Further—although limited to rather small R values—the present work extends the recent *ab initio* computations of Jungen and Jungen [Mol. Phys. **113**, 2333 (2015)] to higher excitation energies which are not accessible to standard quantum-chemical methods. Where a comparison with the calculations of Jungen and Jungen and other older results can be made, namely for $n \leqslant 5$, very good agreement with previous *ab initio* results is obtained.

DOI: 10.1103/PhysRevA.94.022516

I. INTRODUCTION

The hydrohelium ion, HeH^+, is thought to be the first molecular species to have appeared in the universe, possibly along with $He_2{}^+$ [1]. According to the big-bang model, stars formed from primordial material should contain HeH^+, which therefore could influence their formation and evolution. Dabrowski and Herzberg, in 1977, suggested that HeH^+ could exist in astrophysical environments [2]. However, many years elapsed before the vibration-rotation spectrum [3,4] and pure rotation spectrum [5] could actually be observed in the laboratory, while even today HeH^+ has not yet been detected in outer space.

The hydrohelium ion is the simplest and lightest heteronuclear system possessing more than a single electron, which makes this ion interesting also for theoretical studies. The system of excited states of HeH^+ qualitatively resembles that of $H_2{}^+$ [6], with a bound ground state and mostly dissociative excited states, some of which possess shallow minima at relatively large internuclear separations.

Following earlier quantum-chemical computations, such as, e.g., the work of Kołos [7], Pachucki and Komasa published state-of-the-art *ab initio* calculations of the electronic ground state of HeH^+ that take account of nonadiabatic, relativistic, and quantum electrodynamics effects [8]. Previous *ab initio* work on the excited states of HeH^+ includes the early series of papers by Green *et al.* [9–12], which were motivated primarily by the interest in low-energy $H^+ + He$ and $H + He^+$ charge-exchange collisions. These authors performed a CI (configuration interaction) treatment that provided potential-energy curves of $^{1,3}\Sigma$, $^{1,3}\Pi$, and $^{1,3}\Delta$ symmetry states up to $R \approx 40$ bohrs and up to $n = 3$ (where n is the principal quantum number of the outer electron), and they also computed electronic dipole transition moments between these states, as well as nonadiabatic coupling functions. A few years ago Loreau *et al.* [13] recalculated essentially the same data for a larger R range (several hundred bohrs), using the quantum chemistry package MOLPRO [14], and including states up to $n = 4$.

In a recent paper [15] we presented exploratory R-matrix calculations of low-lying Rydberg $nd\delta$ $^1\Delta$ and $^3\Delta$ states in HeH^+. These calculations were based on the so-called R-matrix "halfium code" [16,17] developed initially for the study of diatomic hydrogen H_2. While these computations were restricted to a small range of internuclear distances R (up to 5 bohrs), they gave access to higher n quantum numbers (up to $n \approx 10$) than may be reached by standard quantum chemistry methods. It was found that for $n = 3$ and 4, where earlier computations existed, the R-matrix treatment gave agreement to within $<100\ cm^{-1}$ with the early results of Refs. [9,10], whereas it yielded discrepancies of the order of $2000\ cm^{-1}$ when compared with the results of Ref. [13]. These findings have been confirmed by the very recent quantum-chemical computations of Ref. [6]. Here we present extended R-matrix computations. These include now all symmetries up to $^{1,3}\Gamma$ and are based on substantially larger angular and radial basis sets than the calculations of Ref. [15]. We find satisfactory agreement with the calculations of Ref. [6] in all cases. At the same time we have obtained a complete set of states up to $n \approx 10$, and we have also computed scattering states $HeH^{2+} + e^-$ in the electronic continuum.

II. THEORY

A. General considerations

Over the past decade we have developed an *ab initio* R-matrix approach [16] which enables bound states and core-excited scattering states of two-electron systems to be calculated for fixed nuclei. Our work starts out from the ideas of Greene and Yoo [18], which it adapts and extends so as to yield quantum defect matrices that evolve smoothly throughout the bound and continuous energy regions, and which also

vary reasonably mildly as functions of the molecular geometry (internuclear distance R). The "halfium model" combines the variational eigenchannel R-matrix method [19] with the generalized multichannel quantum defect theory (GMQDT) [20], implemented using prolate spheroidal electron coordinates (ξ,η,ϕ) that replace the more familiar spherical coordinates (r,θ,ϕ). This approach has been applied primarily to diatomic hydrogen H_2, where it has been used to investigate the *ungerade* [16,21] and *gerade* [22] singlet symmetries of H_2, as well as the *gerade* triplet [23] and the *gerade* and *ungerade* ${}^{1,3}\Sigma^-$ channels [17].

The R-matrix scheme leads to a global analysis of the electronic interactions active in the molecular compound, as no distinction is made between "open" and "closed" channels at the outset, but instead all channels are treated on the same footing irrespective of their channel thresholds. In this picture core-excited states are included explicitly as electron-ion collision channels in their own right.

In the halfium model, the two-electron configuration space is divided into two regions: (i) a reaction volume where the variational R-matrix method is employed, and (ii) the remaining space, called asymptotic zone, where GMQDT is used. The connection of the inner zone and outer zone wave functions then yields the desired reaction matrix or equivalent quantum defect matrix. In the inner zone the full nonrelativistic two-electron Hamiltonian is taken into account, whereas in the asymptotic zone the single escaping electron is assumed to move in the field of two effective fractional point charges $Z_1^{\rm eff}$ and $Z_2^{\rm eff}$ separated by R, with $Z_1^{\rm eff}+Z_2^{\rm eff}=Z_c$, where Z_c is the total charge of the core. This "halfium" representation of the asymptotic field is more realistic than the spherical Coulomb field with $Z=Z_c$ which is commonly used in R-matrix calculations. This is because the effective charges provide a reasonable approximation to the nonspherical field of the ion core, and in particular to its dipole and quadrupole components [15,24].

B. Formalism

The reaction zone is defined by a preselected value ξ_0 of the spheroidal radial coordinate ξ. ξ_0 typically is chosen to vary with the molecular geometry R. The electronic wave function inside the reaction volume is set up as an expansion over two-electron configurations $\overline{y}_{ij}(\vec{r_1},\vec{r_2})$ as

$$\overline{\Psi}_\beta(E)=\sum_{ij}c_{ij}^{(\beta)}(E)\,\overline{y}_{ij}, \tag{1}$$

where E is the given total energy, and $\vec{r_1}$ and $\vec{r_2}$ are the position vectors of the electrons. The expansion coefficients $c_{ij}^{(\beta)}(E)$ are the result of the variational calculation, with β a solution index. In the variational R-matrix scheme each eigensolution $\overline{\Psi}_\beta(E)$ is characterized by a stationary logarithmic derivative b_β on the reaction surface $\max(\xi_1,\xi_2)=\xi_0$. The two-electron configurations $\overline{y}_{ij}$ are properly symmetrized products of one-electron functions i and j as detailed in Refs. [16,17].

Each one-electron basis function $|i\rangle=|n_i\tilde{\ell}_i\lambda_i\rangle$, confined to the reaction volume, is separable in spheroidal coordinates (ξ,η,φ) and has the form

$$\begin{aligned}\Phi_i(\vec{r})=\langle\vec{r}\,|i\rangle&=\frac{\chi_i(\xi)}{\sqrt{\xi^2-1}}\frac{\zeta_i(\eta)}{\sqrt{1-\eta^2}}\frac{1}{\sqrt{2\pi}}\theta_i(\phi)\\&\equiv\frac{\chi_i(\xi)}{\sqrt{\xi^2-1}}\tilde{Y}_{\tilde{\ell}_i,\pm\lambda_i}(\eta,\phi).\end{aligned} \tag{2}$$

Here, $\tilde{\ell}_i$ is the generalized orbital angular momentum quantum number arising when spheroidal coordinates are used [16]. The factors $\tilde{Y}_{\tilde{\ell}\lambda}(\eta,\phi)$ on the second line of Eq. (2) thus are normalized spheroidal harmonics, analogous to the familiar spherical harmonics (see [24] for the definitions and numerical implementation that we use; in the following we shall omit the tilde on ℓ, but unless stated specifically, ℓ refers to the spheroidal quantum number). Specifically, the azimuthal, angular, and radial parts of each one-electron function $\Phi_i(\vec{r})$ are, respectively, solutions of the following second-order differential equations:

$$\begin{aligned}\left[\frac{d^2}{d\phi^2}+\lambda_i^2\right]\theta_i(\phi)&=0,\\\left[\frac{d^2}{d\eta^2}+k_\eta^2(E,R,\eta)\right]\zeta_i(\eta)&=0,\\\left[\frac{d^2}{d\xi^2}+k_\xi^2(E,R,\xi)\right]\chi_i(\xi)&=0,\end{aligned} \tag{3}$$

where the squared quantum angular and radial momenta are

$$\begin{aligned}k_\eta^2(E,R,\eta)&=\frac{(Z_1-Z_2)R\eta-p^2\eta^2-A}{1-\eta^2}+\frac{\lambda_i^2-1}{(1-\eta^2)^2},\\k_\xi^2(E,R,\xi)&=\frac{(Z_1+Z_2)R\xi-p^2\xi^2+A}{\xi^2-1}+\frac{1-\lambda_i^2}{(\xi^2-1)^2},\end{aligned} \tag{4}$$

with $p^2=-\frac{R^2E}{2}$. In Eq. (4), A is the separation constant which depends on the total energy E, and R is the bond length, while Z_1 and Z_2 are the nuclear charges. The expressions (4) bring out the analogy between the angular (η) and radial (ξ) equations, particularly obvious here since they are written for a heteronuclear molecule with $Z_1\neq Z_2$.

The variational R-matrix approach requires the basis of two-electron functions $\overline{y}_{ij}$ used in the expansion Eq. (1) to consist both of "closed" functions whose radial component $\chi^{(c)}(\xi_0)$ in Eq. (2) vanishes on the reaction surface, as well as of "open" functions whose radial component $\chi^{(o)}(\xi_0)$ is nonzero, but has a vanishing radial derivative on the reaction surface [16]. Each solution $\overline{\Psi}_\beta$ Eq. (1) may then be continued into the external zone, for radii of the outer electron larger than ξ_0, as a linear combination of regular and irregular two-center Coulomb radial functions,

$$\begin{aligned}\overline{\Psi}_\beta(E,\omega,\xi\geqslant\xi_0)=&\frac{1}{\sqrt{\xi^2-1}}\sum_k\overline{\Phi}_k(E,\omega)\\&\times[f_k(\epsilon_k,\xi)I_{k\beta}(E)-g_k(\epsilon_k,\xi)J_{k\beta}(E)].\end{aligned} \tag{5}$$

Here, E is the total energy as before, while $\epsilon_k=E-E_k^+$ is the energy of the outer electron with respect to the state E_k^+ of the residual core corresponding to the channel k and for the given R value. $\overline{\Phi}_k(\omega)$ are so-called "surface harmonics"—essentially

core wave functions coupled together with the angular factor of the escaping electron—for each asymptotic channel k and for each solution β, where ω stands for all coordinates except the radial coordinate of the outermost electron. The form of these surface harmonics as well as their symmetrization and normalization is detailed in Refs. [16,17].

The regular and irregular radial channel functions f_k and g_k that occur in Eq. (5) are solutions of the radial Schrödinger equation of the one-electron two-center Coulomb problem with effective charges $Z_1^{\rm eff}$ and $Z_2^{\rm eff}$ (where $Z_1^{\rm eff} + Z_2^{\rm eff} = Z_1 + Z_2 - 1$). In the previous applications to the H_2 molecule the only reasonable choice of the charges was $Z_1^{\rm eff} = Z_2^{\rm eff} = 1/2$ (hence the name "halfium" model), because in a neutral system we also must have $Z_1^{\rm eff} + Z_2^{\rm eff} = Z_c = 1$ (with Z_c the total core charge), and the inversion symmetry must be preserved. In the dipolar system HeH^+ we must have $Z_1^{\rm eff} + Z_2^{\rm eff} = Z_c = 2$, but various choices of the effective charges are now possible as will be discussed in Sec. III below.

The summation index k in Eq. (5) runs over those channels $k \equiv i'j'$ that are taken into account explicitly in the asymptotic zone. The matching of the outer and inner eigensolutions, Eqs. (5) and (1), respectively, yields the coefficient matrix elements $I_{k\beta}$ and $J_{k\beta}$ that appear on the right-hand side of Eq. (5); see Refs. [16,17] for a detailed description of the matching procedure. Finally, the short-range reaction matrix is obtained according to $\mathbf{K} = \mathbf{JI}^{-1}$. This matrix contains, in compact form, the information on the intra- and interchannel interactions that take place inside the reaction volume. It provides the input to the MQDT routines used to compute the energies of the bound states, and also the positions and widths of core-excited resonances.

C. Bound levels

Bound states are determined by setting up the MQDT secular equation:

$$\det|\tan\beta_k(\epsilon_k)\delta_{kk'} + K_{kk'}(E)| = 0, \tag{6}$$

which is solved separately for each $R-$value and total energy E, and yields discrete electronic eigenenergies $E_n(R)$ for arbitrarily high n values. The accumulated phase parameters of generalized multichannel quantum defect theory, $\beta_k(\epsilon_k)$, are evaluated using the procedures given in Ref. [20]. The quantity β_k/π measures the number of radial half wavelengths that "fit" into the asymptotic potential at the given channel energy ϵ_k. The eigenenergies $E_n(R)$ are converted into potential-energy curves $U_n(R)$ by adding the internuclear repulsion energy. Finally, effective quantum number functions $n^*(R)$ may be derived by means of the one-channel Rydberg equation (written here in atomic units):

$$n^*(R) = \frac{Z_c}{\sqrt{2[E^+_{k=1}(R) - E_n(R)]}}, \tag{7}$$

where $Z_c = 2$, appropriate for HeH^+, is the net charge experienced by the outermost electron, and $E^+_{k=1}$ is the ionization threshold. Since the $k = 1$ HeH^{2+} ground state has $^2\Sigma^+$ symmetry, the $^{1,3}\Lambda$ Rydberg channels of HeH^+ are conveniently labeled as $\epsilon\ell\lambda$ with $\lambda = \Lambda$, while $n\ell\lambda$ approximately labels the individual Rydberg states as long as channel mixing is not very strong.

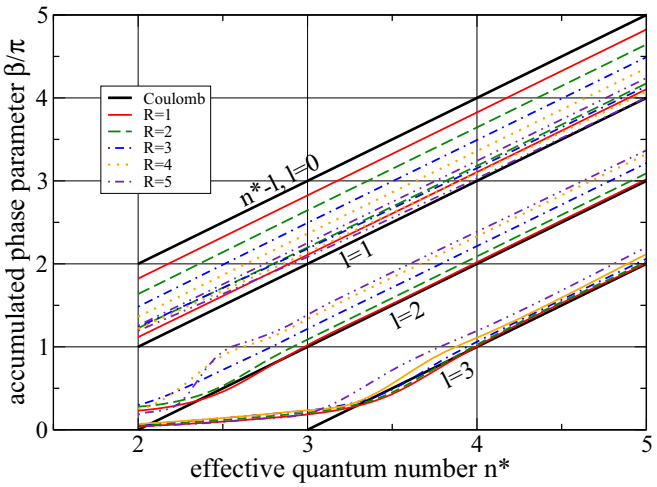

FIG. 1. Accumulated spheroidal phase parameters β/π for $Z_1 = Z_2 = 1$, $\ell,\lambda = 0$ ($\ell = 0-3$), and various R values, plotted as functions of n^* which is related to the energy by Eq. (7). The Coulomb reference phases are represented by thick lines and correspond to $n^* - \ell$. The phase parameters of the two-center system are represented by thin lines with color coding as indicated in the figure.

The quantity $n^*(R) - \ell$, with n^* evaluated according to Eq. (7) is in fact the analog of the phase parameter $\beta_{k=1}/\pi$ of Eq. (6) for a spherical Coulomb field. It is thus of interest to compare the Coulomb phase parameter with the the two-center parameter implied by Eq. (6). Figure 1 illustrates this for $\lambda = 0$. The figure is a plot of the spherical Coulombic (thick lines) and the spheroidal two-center (thin lines) accumulated phase parameters versus n^*. The plot shows how, apart from the lowest energies corresponding to $n^* \leqslant \ell + 1$, the differences $\beta/\pi - n^* + \ell$, while depending on the geometry R, have essentially constant values as functions of the excitation energy. These differences account for the R-, energy-, and $\ell\lambda$- dependent contributions to the quantum defect that stem from the two-center nature of the asymptotic field in which the electron is moving once it has escaped from the core region. The figure also shows that as ℓ increases, the difference between the Coulombic and the two-center accumulated phase parameter values decreases. The role of the inner-zone variational R-matrix calculation is to account for the deviations from two-center-like behavior, namely exchange effects between the two electrons and the increased nuclear attraction in the vicinity of the He nucleus [25].

III. DETAILS OF CALCULATIONS

The main parameters determining an R-matrix calculations are (i) the choice of the reaction volume ξ_0 for any given R value. (ii) the radial and angular basis set (configuration functions $\overline{y}_{ij}$) used inside the reaction zone, (iii) the number of channel functions (partial-wave expansion), (iv) the number of core states explicitly included in the external zone, (v) the choice of the effective charges $Z_1^{\rm eff}$ and $Z_2^{\rm eff}$, the sum of which must equal $Z_c = 2$, the core charge. The present R-matrix calculations have been improved and optimized in

TABLE I. $^1\Delta$ states of HeH^+ for $R = 4$ a.u.: choice of external ℓ basis.

State	*ab initio* Ref. [6]	*R* matrix, $\ell_{max} = 3$ Ref. [15]	ΔU	*R* matrix, $\ell_{max} = 5$ Present	ΔU
$3d\delta$	−1.94500[a]	−1.94509	20[b]	−1.94508	18
$4d\delta$	−1.86385	−1.86401	35	−1.86392	15
$5d\delta$	−1.82455	−1.82462	15	−1.82462	15
$4f\delta$	−1.87510	−1.87306	−448	−1.87516	13
$5f\delta$	−1.83025	−1.82924	−222	−1.83030	11
$5g\delta$	−1.83113			−1.83117	9

[a]Total energy $U_n(R = 4)$ in a.u.
[b]ΔU, difference *ab initio*, *R* matrix, in cm^{-1}.

TABLE II. $^1\Delta$ states of HeH^+ for $R = 4$ a.u.: choice of core state basis.

State	*ab initio* Ref. [6]	*R* matrix Core $1s\sigma$	ΔU	*R* matrix Core $1s\sigma, 2p\sigma$	ΔU
$3d\delta$	−1.94500[a]	−1.945080	18[b]	−1.945086	19
$4d\delta$	−1.86385	−1.863921	16	−1.863923	16
$5d\delta$	−1.82455	−1.824619	15	−1.824619	15
$4f\delta$	−1.87510	−1.875157	13	−1.875158	13
$5f\delta$	−1.83025	−1.830296	10	−1.830297	10
$5g\delta$	−1.83113	−1.831170	9	−1.831170	9

[a]Total energy $U_n(R = 4)$ in a.u.
[b]ΔU, difference *ab initio*, *R* matrix, in cm^{-1}.

several respects as compared to our preliminary computations of Ref. [15], as we now describe. In order to illustrate the optimization procedures we shall in the following use the quantum-chemical computations of Ref. [6] as reference calculations.

(i) Choice of ξ_0. It has been customary [18] to parametrize the R dependence of the reaction boundary as

$$\xi_0 = 1 + C/R, \tag{8}$$

defining an ellipsoid with a major axis equal to $R + C$. The parameter C must be chosen such that the electronic wave function of the residual core, HeH^{2+} in our case, is fully contained inside the volume for all R values considered, in such a way that the eigenvalue of the confined state differs from the free state by less than a preselected small value. At the same time it is desirable to keep ξ_0 as small as possible in order to minimize the energy dependencies of the quantum defects or reaction matrices. We have found that the choice of $C = 12$ a.u. in Eq. (8) is satisfactory as it yields the $1s\sigma$ and $2p\sigma$ HeH^{2+} core states correctly to within $<10\,cm^{-1}$. By contrast, with the choice $C = 10$ bohrs, for instance, the confined $2p\sigma$ core state is shifted to higher energy by $\geqslant 20\,cm^{-1}$.

(ii) As compared to our previous work [15], the inner-zone basis sets have been increased from about 300 two-electron functions up to 1000 functions.

(iii) The outer zone angular basis included partial waves up to $\ell = 5$ instead of 3 previously. Table I illustrates the effect of this for the lowest $^1\Delta$ states. Inclusion of two more partial-wave components is seen to improve the $\ell = 3$ state energies substantially, whereas the $\ell = 2$ states are just very slightly improved. We have verified that a further increase of the basis to $\ell_{max} = 7$ changes the results by $\ll 1\,cm^{-1}$.

(iv) We have found that in the energy range explored here, and unlike in H_2, it is not necessary to explicitly include core-excited channels in the outer zone. The data presented in Table II demonstrate this: explicit inclusion of the channels associated with the $2p\sigma$ core state systematically lowers the Rydberg energies somewhat, but in fact by less than $\approx 1 cm^{-1}$ in all cases.

This behavior is in contrast to H_2, where the inclusion of core-excited channels is known to be crucial. Figure 2 compares the ground state and excited core states for the two molecules. The $1s\sigma$ and $2p\sigma$ states are seen to remain widely separated in HeH^{2+} over the range of R values shown, whereas in $H_2{}^+$ they quickly coalesce as R increases. The different dissociation behavior of the $1s\sigma$ and $2p\sigma$ states in the two one-electron core ions is required by the different correlation rules for molecules with equal or unequal nuclear charges [26]. The qualitatively different behavior of the core states carries over into the Rydberg manifolds associated with them (broken lines in Fig. 2), with the result that core excited configurations in HeH^+ interact only weakly with ground-state Rydberg configurations. In view of these considerations and the results shown in Table II, we have therefore omitted core-excited channels in our description of the wave functions in the asymptotic zone.

The basis set choices for the asymptotic zone just described yield quantum defect or reaction matrices of dimension $\ell_{max} + 1 - \lambda$, i.e., 6×6 matrices for $^{1,3}\Sigma^+$ symmetry, and correspondingly reduced dimensions for larger values of $\lambda = \Lambda$.

(v) The distribution of the total ion core charge $Z_c = 2$ on the two centers is in principle arbitrary, as any converged calculation should yield the same result whatever choice has been made. However, the ℓ-mixing channel interactions will be different and the convergence properties may not be the same.

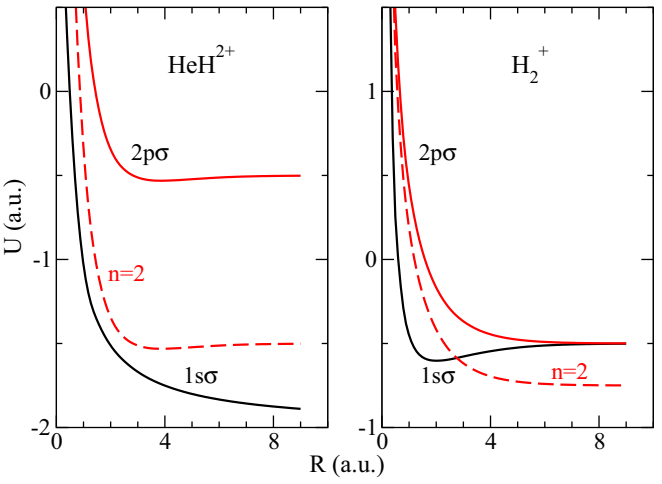

FIG. 2. The ground- and first excited-state potential-energy curves of HeH^{2+} (left) (after Winter *et al.* [27]) and $H_2{}^+$ (right): full lines. Rydberg potential-energy curve associated with the excited-state ion curve and corresponding to $n = 2$: broken lines.

The following arguments suggest the choice $Z_1^{\rm eff} = Z_2^{\rm eff} = 1$ which we have adopted: First, the work of Ref. [6] highlighted the similarities between the electronic level structures of HeH^+ and of $H_2{}^+$, which stem from the fact that the He^+ ground-state ion with its tightly bound $(1s)$ electron effectively acts in a good approximation like a singly charged point charge. Therefore it is natural to represent the ion core HeH^{2+} by two equal point charges as in $H_2{}^+$. Further, if the effective charges are distributed in such a way that at very large distance ξ from the core the outermost electron sees a double point charge situated on the center of charge of the ion core, the dipole component of the longe-range field vanishes [28], and therefore dipolar channel couplings are minimized and the convergence is faster. This choice is dependent on the internuclear distance R, but since HeH^{2+} quickly approaches the configuration $He^+ + H^+$, the center of charge will be near the midpoint between the two nuclei, implying once again $Z_1^{\rm eff} = Z_2^{\rm eff} = 1$. Finally, we have verified by means of test calculations in which the choices $Z_1^{\rm eff} = 8/5$ and $Z_2^{\rm eff} = 2/5$, or alternatively $Z_1^{\rm eff} = 4/3$ and $Z_2^{\rm eff} = 2/3$ were made (cf. the discussion given in Ref. [15]), that the convergence was indeed substantially slower than when $Z_1^{\rm eff} = Z_2^{\rm eff} = 1$ was taken.

It is not straightforward to provide an *a priori* estimate of the accuracy of our calculations, in particular because only comparatively few computations of bound states using R-matrix methods have been made in the past, cf. the reviews by Aymar *et al.* [29] and Tennyson [30]. However—in the absence of experimental results for excited HeH^+—we can obtain an approximate estimate of the accuracy by comparing our data with available *ab initio* results where these exist. The energies given in Tables I and II are seen to differ from the quantum-chemical results of Ref. [6] in the fifth digit after the decimal point. We have therefore chosen to quote our results—n^* values and energies—with five digit accuracy throughout, although it shall turn out below (cf. Table V, Sec. IV A) that in some cases the differences with respect to Ref. [6] are up to two orders of magnitude larger.

Further justification for quoting our results with five digit accuracy is based on the following arguments: As the R-matrix computations initially provide phase shifts rather than energies—the latter are obtained only in the subsequent MQDT calculations—it is reasonable to assume that the phase-shift accuracy varies little along a given Rydberg series. The relationship between the energy and the effective principal quantum numbers on the other hand is highly nonlinear, as it scales, in cm^{-1}, according to

$$\Delta U_n = \frac{2Z_c^2\mathcal{R}}{n^{*3}}\Delta n^*, \tag{9}$$

with $\mathcal{R}$ the Rydberg constant. By systematically quoting our calculated n^* values with five figures after the decimal point, we avoid rounding-off errors $\geqslant 1\,cm^{-1}$ resulting from the use of Eq. (9) for any n value along any given Rydberg series, when converting phase shifts into energies. This is the case irrespective of the real accuracy of the effective principal quantum numbers. Logically, the energies are given with the same number of digits (with the exception of the ion limits, Table III below, which should be accurate to one more significant figure). As already mentioned we shall find below (Table V, Sec. IV A) that the actual accuracy of our calculated n^* values is probably up to two orders of magnitudes less.

TABLE III. HeH^{2+} ground-state electronic energies (a.u.).

R	$E_{k=1}{}^+$
1	−3.033355
2	−2.512195
3	−2.335549
4	−2.250605
5	−2.200235

IV. RESULTS AND DISCUSSION

A. Comparison with previous work

For energies in the discrete range our calculations yield total electronic energies $E_n(R)$. Following our own earlier work [16] and also that of Ref. [6], we prefer here to convert the energies into effective principal quantum numbers $n^*(R)$ by means of the Rydberg equation Eq. (7) with $Z_c = 2$. The HeH^{2+} one-electron ion core energies $E_{k=1}{}^+$ required to evaluate Eq. (7) were computed by direct numerical integration of Eqs. (3) with $Z_1 = 2$, $Z_2 = 1$. They are listed in Table III. The advantage of the n^* values is that they provide a direct measure of the effective electron-ion scattering phase. Indeed, one has $n^*(\mathrm{mod}1) = -\mu_{\rm eff}$, where $\mu_{\rm eff}$ is the effective phase shift or quantum defect with reference to a pure Coulomb field. The interpretation of the results in terms of Rydberg series is thus straightforward. Table IV lists our results for singlet and triplet Σ^+ states, for n values up to 6 for which the comparison with the results of Ref. [6] is possible. Note that the assignments given in the table have only a limited meaning and serve primarily for bookkeeping purposes, as all the series are mixed to some extent. The table lists n^* values for the singlet states as well as the singlet-triplet differences $\Delta n^*(s-t) = n^*(\mathrm{singlet}) - n^*(\mathrm{triplet})$. For each of these entries, the difference with respect to the equivalent data from Ref. [6] is given. The rms deviation between our 90 singlet n^* values listed in the table and those of Ref. [6] is -0.0018 ± 0.0026, which is very good agreement. This is nearly an order of magnitude better than what we achieved previously for H_2 [16,22], and more than ten times better than what Greene and Yoo [18] envisioned—again for H_2—necessary to obtain a meaningful quantitative description of the Rydberg physics in a diatomic molecule.

Analogous tables for the ${}^{1,3}\Pi$, ${}^{1,3}\Delta$, ${}^{1,3}\Phi$, ${}^{1,3}\Gamma$ symmetries may be found in the Supplemental Material associated with the present paper [31]. The mean deviations between the *ab initio* and the R-matrix n^* values for all the symmetries are collected in Table V, which shows that the quantum-chemical and the R-matrix results are equally consistent for all symmetries. Figure 3 displays the values $n^*(\mathrm{mod}\ 1)$ as functions of R for singlet Σ^+, Π, and Δ symmetry (upper panels) as well as the corresponding singlet-triplet splittings (lower panels). Starting from the united-atom limit ($R = 0$), the n^* values evolve as closely spaced families of curves corresponding each to a specific value $\ell\lambda$. The close spacings highlight the

TABLE IV. Effective principal quantum numbers n^* for $^{1,3}\Sigma^+$ states of HeH^+ R = internuclear distance in a.u., n^* = effective principal quantum number evaluated with Eq. (7) for the singlet component. $\Delta n^*(s-t) = n^*(\text{singlet}) - n^*(\text{triplet})$. All n^* values are given with five-digit accuracy, but the actual accuracy could be up to two orders of magnitude less; cf. comments in the text.

	n^*	Ref. [6] - col. 1	$\Delta n^*(s-t)$	Ref. [6] - col. 3	n^*	Ref. [6] - col. 5	$\Delta n^*(s-t)$	Ref. [6] - col. 7
R/a.u.	1	2	3	4	5	6	7	8
	$^{1,3}\Sigma^+$							
	$2s\sigma$				$3p\sigma$			
1	2.13151	−0.00411	0.11313	−0.00392	2.86608	−0.00450	0.16191	−0.00486
2	2.31897	−0.00306	0.10050	−0.00250	2.72020	−0.00391	0.10210	−0.00411
3	2.46586	−0.00410	0.10036	0.00563	2.71875	−0.00545	0.12184	−0.00633
4	2.54246	−0.00992	0.17082	−0.01229	2.65204	−0.00153	0.07603	0.00046
5	2.48129	−0.00070	0.14687	−0.01502	2.72469	−0.00200	0.08097	−0.00124
	$3d\sigma$				$3s\sigma$			
1	2.97245	0.00018	0.00568	0.00015	3.13914	−0.00756	0.10476	−0.00381
2	2.90583	−0.00115	0.03679	−0.00083	3.32895	−0.00508	0.08913	−0.00247
3	2.80119	−0.00222	0.05594	−0.00216	3.47997	−0.00358	0.09092	−0.00328
4	2.81292	−0.00117	0.04335	−0.00172	3.56617	−0.00464	0.13760	−0.00556
5	2.87215	−0.00405	0.03940	−0.00632	3.53019	−0.00003	0.12003	−0.00481
	$4p\sigma$				$4d\sigma$			
1	3.86377	−0.00222	0.15374	−0.00810	3.96720	0.00513	0.00588	0.00141
2	3.73964	−0.00234	0.10219	−0.00655	3.90500	−0.00200	0.04260	−0.00015
3	3.73179	−0.00410	0.13116	−0.00570	3.82156	−0.00429	0.05208	−0.00359
4	3.65955	−0.00080	0.06018	−0.00036	3.86168	−0.00144	0.04548	−0.00200
5	3.74490	−0.00223	0.05090	−0.00111	3.80645	−0.00053	0.02291	0.00153
	$4f\sigma$				$4s\sigma$			
1	3.99709	−0.00505	0.00096	−0.00091	4.14094	−0.00807	0.10085	−0.00278
2	3.97175	−0.00071	0.00015	0.00027	4.33179	−0.00526	0.08560	−0.00265
3	3.93638	0.00040	0.00205	0.00049	4.48404	−0.00156	0.08470	−0.00268
4	3.88660	−0.00008	0.01129	0.00034	4.57712	−0.00359	0.12900	−0.00493
5	3.93542	−0.00206	0.04637	−0.00189	4.55561	−0.00326	0.11714	−0.00476
	$5p\sigma$				$5d\sigma$			
1	4.86299	−0.00114	0.14923	−0.00814	4.96756	0.00476	0.00655	0.00133
2	4.74827	−0.00218	0.10182	−0.00698	4.90444	−0.00227	0.04453	−0.00005
3	4.73511	−0.00406	0.13191	−0.00598	4.83255	−0.00456	0.05142	−0.00410
4	4.66252	0.00016	0.05519	−0.00042	4.87349	−0.00074	0.03661	−0.00139
5	4.75040	−0.00282	0.04205	−0.00188	4.80016	−0.00042	0.03229	0.00238
	$5f\sigma$				$5g\sigma$			
1	4.99259	−0.00036	0.00075	−0.00066	5.00059	−0.00346	0.00020	−0.00020
2	4.97047	0.00038	0.00026	0.00041	4.98858	−0.00029	0.00004	−0.00004
3	4.93601	0.00002	0.00446	−0.00055	4.97337	−0.00024	0.00007	−0.00004
4	4.89426	−0.00097	0.02579	−0.00025	4.95202	−0.00016	0.00003	0.00009
5	4.92383	−0.00021	0.00926	−0.00039	4.96407	−0.00220	0.04046	−0.00197
	$5s\sigma$				$6p\sigma$			
1	5.14187	−0.00809	0.09914	−0.00220	5.86273	−0.00027	0.14672	−0.00795
2	5.33275	−0.00439	0.08359	−0.00218	5.75264	−0.00209	0.10160	−0.00687
3	5.48582	−0.00120	0.08171	−0.00274	5.73650	−0.00407	0.13194	−0.00623
4	5.58246	−0.00339	0.12499	−0.00486	5.66401	0.00019	0.05307	−0.00039
5	5.56662	−0.00260	0.11617	−0.00528	5.75218	−0.00230	0.03811	−0.00285
	$6d\sigma$				$6f\sigma$			
1	5.96771	0.00492	0.00689	0.00130	5.99108	0.00156	0.00067	−0.00056
2	5.90409	−0.00220	0.04529	0.00003	5.96999	0.00093	0.00041	0.00039
3	5.83874	−0.00459	0.05129	−0.00411	5.93547	0.00042	0.00519	−0.00044
4	5.87459	−0.00016	0.02687	−0.00064	5.90331	−0.00127	0.03840	−0.00068
5	5.79726	−0.00028	0.03595	0.00339	5.92296	0.00058	0.00060	0.00002
	$6g\sigma$				$6h\sigma$			
1	5.99843	0.00041	0.00001	0.00112	6.00152	−0.00090	0.00020	0.00093
2	5.98856	0.00016	0.00002	−0.00002	5.99384	0.00026	0.00001	−0.00001
3	5.97308	0.00018	0.00003	0.00002	5.98619	−0.00010	0.00007	−0.00007
4	5.95158	0.00032	0.00011	0.00005	5.97549	−0.00041	−0.00006	0.00006
5	5.96216	−0.00116	0.03399	0.00409	5.97947	−0.00252	0.01742	

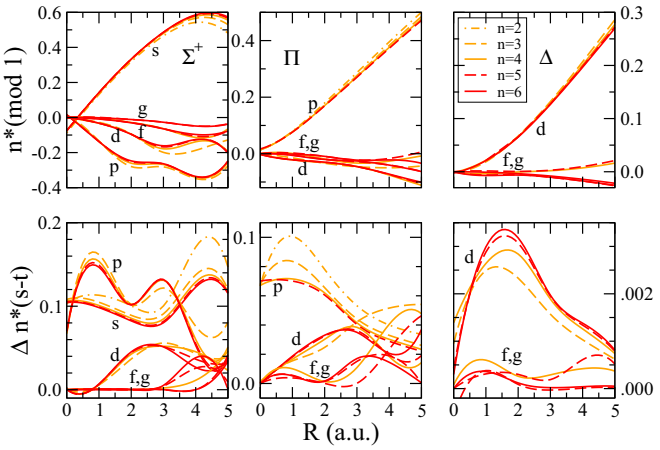

FIG. 3. Effective quantum defects, $-\mu_{\rm eff} = n^*$ [mod(1)], for singlet components (top panels) and singlet-triplet splittings Δn^*(s-t) (bottom panels) for Σ^+, Π, and Δ states (from left to right) in HeH$^+$, as functions of the internuclear distance R and for various values n, $2 \leqslant n \leqslant 6$. Different n values are distinguished by different colors and line styles as indicated in the figure. The values for $R = 0$ (Li$^+$) have been calculated based on the compilation of Moore [32].

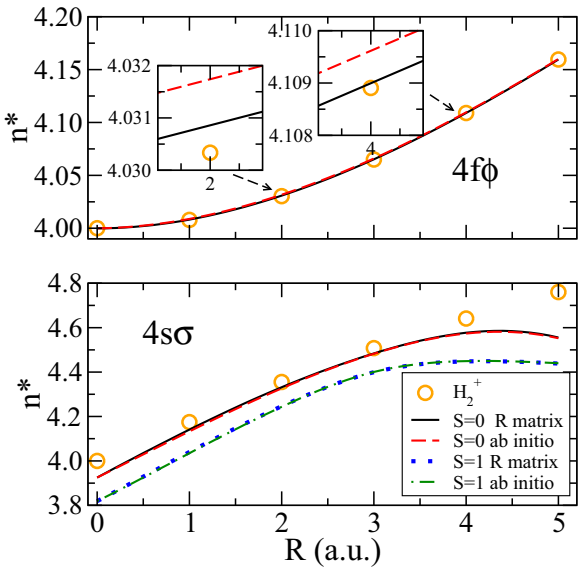

FIG. 4. Effective principal quantum numbers n^* for the $4f\phi$ (top) and $4s\sigma$ (bottom) states of HeH$^+$, plotted as functions of the internuclear distance R. The R-matrix results (full lines and dotted lines) are compared with the quantum-chemical results from Ref. [6] (dashed lines and dot-dashed lines), as well as with the values for the H_2^+ ion (circles). Upper panel, insets: enlarged sections near $R = 2$ and 4 a.u. The calculated singlet-triplet splitting is not visible on the scales used in the figure and has therefore been omitted. Lower panel: The singlet-triplet splitting is well developed and significant deviations from H_2^+ are apparent.

near constancy with energy of the effective quantum defect. As the internuclear distance increases, this simplicity gets lost to some extent, owing, in part, to the fact that ℓ-mixing interactions occur, but also because the effective core charge seen by the excited electron starts to change from 2 to 1 as has been discussed in Ref. [6]. The effective quantum defects $\mu_{\rm eff} = -n^*$(mod 1) nevertheless are seen to exhibit overall a more or less smooth behavior.

B. Nonpenetrating versus penetrating states

Figure 4 (upper panel) illustrates the effective principal quantum number n^* and its evolution with R for a high-ℓ, high-λ state, $4f\phi$. Owing to the high orbital angular momentum values, the Rydberg electron is effectively kept away from the nuclei, that is, it has *nonpenetrating* character, with the result that the screening of the doubly charged He nucleus by the $1s$ electron should be complete. We therefore expect the HeH$^+$ $4f\phi$ state to behave very nearly like its counterpart in H_2^+. Figure 4 shows that this is indeed the case. The theoretical HeH$^+$ values are indistinguishable on the global scale of the figure from those of H_2^+, and it is only in the blown-up sections shown for $R = 2$ and $R = 4$ that differences of the order of 10^{-3} become visible. It appears unlikely, however, that these small differences have any physical significance. They may well reflect the conceptual and numerical limits of each of the two theoretical methods which we compare here. Nevertheless it is interesting to note—see Table V—that the R-matrix results for the higher Λ and hence ℓ values correspond systematically to very slightly *lower* energies than the variational quantum-chemical results.

Finally, as a contrast, the lower panel of Fig. 4 displays the same information for the $4s\sigma$ state which belongs to the most strongly penetrating Rydberg series of HeH$^+$. Here the singlet-triplet splitting is seen to be well developed, and the deviations from H_2^+-like behavior are substantial. At the same time, the R matrix and *ab initio* values can hardly be distinguished on the plot. This proves that exchange and penetration effects are taken into account at an equivalent level—and therefore most probably correctly—in the two theoretical approaches.

C. Extension to higher energies

Extensive R-matrix and generalized MQDT computations have been carried out for all symmetries and geometries $1 \leqslant R \leqslant 5$, and up to $n \approx 10$. Detailed tables are given in the Supplemental Material [31] which contains information on nearly 100 electronic states. As an example of these results, Fig. 5 depicts the (negatives of the) effective quantum defects of $^1\Sigma$, $^1\Pi$, and $^1\Delta$ symmetry for $R = 4$ a.u., respectively, as functions of the Rydberg energy $\epsilon = -Z_c^2/n^{*2}$. The plots span the energy range from $n = 5$ or 6, values for which the highest *ab initio* values have been obtained, up to $n \approx 10$–11. Our

TABLE V. Mean deviations *ab initio*, R matrix.

	Number of data points	*ab initio*, R matrix	
		Δn^*(singlet)	Singlet-triplet splitting
Σ^+	90	-0.002 ± 0.003	-0.002 ± 0.003
Π	60	-0.001 ± 0.002	-0.001 ± 0.002
Δ	30	$+0.0001 \pm 0.0001$	$+0.00003 \pm 0.0002$
Φ	15	$+0.0006 \pm 0.0004$	$+0.00000 \pm 0.00001$
Γ	15	$+0.0008 \pm 0.0006$	-0.000001 ± 0.000003

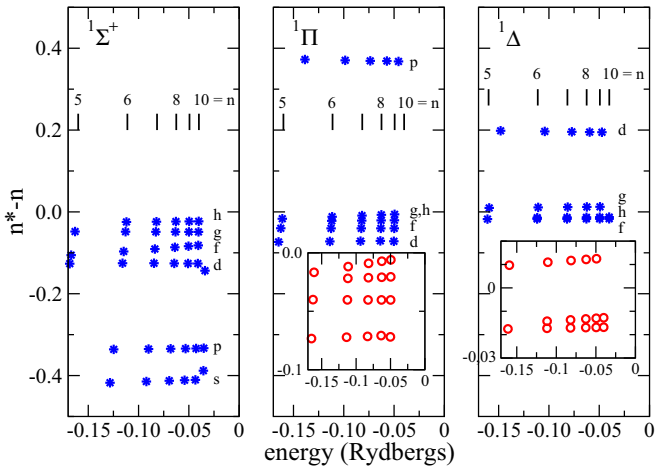

FIG. 5. Calculated higher Rydberg states of HeH^+ for $R = 4$ a.u. and $^1\Sigma^+$, $^1\Pi$, and $^1\Delta$ symmetry (from left to right). Values $-\mu_{\rm eff} = n^* - n$ are plotted vs the Rydberg electron binding energy ϵ (in Rydbergs). The energy positions of the He^+ hydrogenic levels are indicated by vertical bars. Insets: enlarged views of the portions near $n^* - n \approx 0$.

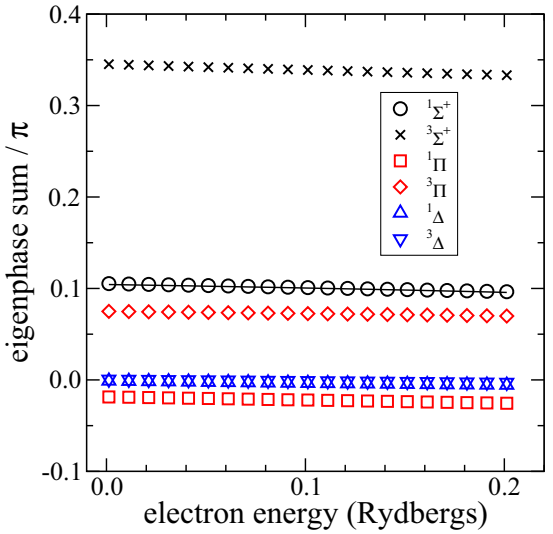

FIG. 6. HeH^{2+}-e^- continuum eigenphase sums (in units of π) for $^{1,3}\Sigma^+$, $^{1,3}\Pi$, and $^{1,3}\Delta$ symmetry, respectively, plotted vs the energy of the continuum electron (in Rydbergs). The plot corresponds to $R = 4$ bohrs. The meaning of the symbols is indicated in the figure. The full line is the result of a $^1\Sigma^+$ calculation where six closed channels $\ell = 0$–5 associated with the $2p\sigma$ excited-state core were included in addition to the six open channels associated with the $1s\sigma$ ground-state HeH^{2+} ion core.

calculations are seen to predict the numerous Rydberg series to evolve quite regularly. Not unexpectedly, the higher ℓ values yield near-zero quantum defects. In addition, interestingly, the higher the value of Λ, the closer we find the series crowded together near the $n^* - n = 0$ line. For $\Lambda = 0$, on the other hand, the various series are clearly spread apart by interseries interactions.

D. Continuum states

The HeH^{2+} - e^- electron-ion continuum scattering phases are derived by use of the secular equation (6), where it suffices to replace, for each open channel k, the closed-channel phase parameter β_k by the negative of the continuum eigenphase, $-\pi\tau$. Equation (6) thereby is converted into an eigenvalue equation that yields eigenphases $\pi\tau_\rho$, $\rho = 1 \ldots N_o$, where N_o is the total number of open continua at energy E (see, e.g., Ref. [33] for a detailed description of this methodology).

Figure 6 displays the eigenphase sums $\sum_\rho \tau_\rho$ for $^{1,3}\Sigma^+$, $^{1,3}\Pi$, and $^{1,3}\Delta$ symmetry, in units of π radians and evaluated for $R = 4$ bohrs, using the same reaction matrices, **K(E)**, that have been employed for the bound-state calculations. The eigenphase sums are seen to exhibit a smooth, almost constant, behavior as functions of the energy, which is in line with the nearly constant effective bound-state quantum defects $\mu_{\rm eff}$ displayed in Fig. 5. It should be noted however that the phase sums plotted in Fig. 6 refer to the two-center spheroidal reaction matrices and thus are not directly comparable to the quantum defects of Fig. 5 which are Coulombic [Eq. (7)]; cf. the discussion in Sec. II C. Not unexpectedly, the singlet-triplet difference of the phase sums is large for Σ^+ symmetry and decreases rapidly as Λ increases.

Inspection of the individual eigenphases indicates that for all symmetries one single eigenphase (two in the case of $^{1,3}\Sigma^+$ symmetry), namely that which corresponds approximately to the lowest ℓ value, differs significantly from zero and thus provides the main contribution to the scattering and hence the phase sum. The minor components are crucial in order to achieve good accuracy in the bound-state calculations as we have seen in Sec. III, but do not seem to play a major role here.

It is well known that the energy derivative of the eigenphase sum exhibits characteristic peaks near autoionization resonances, where in the case of isolated resonances these peaks have a Lorentzian shape. Closed channels associated with the $2p\sigma$ excited HeH^{2+} core are in principle present in the range covered by Fig. 6, although we have excluded them from our calculations based on the arguments given in Sec. III. As an additional check we have carried out a $^1\Sigma^+$ R-matrix and MQDT calculation for $R = 4$ bohrs whereby the $\ell = 0$–5 closed channels associated with the $2p\sigma$ excited-state core were reintroduced in addition to the $\ell = 0$–5 open channels associated with the $1s\sigma$ ground-state core. The result of this calculation is represented by a full line in Fig. 6. It may be seen that on the scale of the figure no difference is visible between the 12-channel (full line) and the six-channel calculation (circles), indicating that resonance effects are negligible in this energy region.

V. CONCLUSION

In the present work we have investigated highly excited electronic states of the hydrohelium ion HeH^+. These results are an extension of the quantum-chemical calculations of Ref. [6] which—while covering a larger range of nuclear geometries than we consider here—were limited to moderate electronic excitation. The region of overlap of the two studies—moderate electronic excitation at small R values—has permitted us to test the accuracy of our R-matrix approach by comparison with the quantum-chemical results.

The comparison is gratifying, as in terms of electron phase shifts the R-matrix data deviate from the quantum-chemical results by less than two parts per thousand in all cases. This level of quantitative agreement represents a substantial improvement, by nearly an order of magnitude, as compared to earlier R-matrix calculations on similar systems, such as H_2 [16,22] or HeH [34], including also our own previous work on HeH^+ [15]. This comparison obviously takes account of the Z scaling between neutral and charged Rydberg systems.

HeH^+ molecules may be formed in the divertor region of fusion reactors such as ITER, and HeH^{2+}-e^- scattering processes could play a role in such plasmas. Comprehensive data on the electronic structure of this ion and related collision processes should therefore be useful in this context [35]. As an extension of this work we plan to compute dipole transition moments from the HeH^+ ground state to its excited states as well as to the ionization continuum.

We are not aware of any previous systematic application of R-matrix theory combined with quantum defect theory to a molecular ion. It has been pointed out in Ref. [6] that a conceptual problem arises as R increases, when MQDT is applied to a system with a doubly charged core. The reason is that upon dissociation the effective core charge is bound to change from 2 to 1, when the excited electron is attached to either one of the singly charged fragments of the core. It is not clear yet at this point how these features can be built into the theory in a satisfactory manner.

ACKNOWLEDGMENTS

C.J. received funding from the E. Miescher Foundation (Basel, Switzerland). We thank Dr. M. Jungen (University of Basel, Switzerland) for his comments on the manuscript and for providing unpublished HeH^+ *ab initio* data.

[1] S. Lepp, P. C. Stancil, and A. Dalgarno, J. Phys. B: At. Mol. Opt. Phys. **35**, R57 (2002).
[2] I. Dabrowski and G. Herzberg, Trans. N. Y. Acad. Sci. Ser. II **38**, 14 (1977).
[3] P. Bernath and T. Amano, Phys. Rev. Lett. **48**, 20 (1982).
[4] A. J. Perry, J. N. Hodges, C. R. Markus, G. S. Kocheril, and B. J. McCall, J. Chem. Phys. **141**, 101101 (2014).
[5] F. Matsushima, T. Oka, and K. Takagi, Phys. Rev. Lett. **78**, 1664 (1997).
[6] M. Jungen and Ch. Jungen, Mol. Phys. **113**, 2333 (2015).
[7] W. Kołos, Int. J. Quantum Chem. **10**, 217 (1976).
[8] K. Pachucki and J. Komasa, J. Chem. Phys. **137**, 204314 (2012).
[9] T. A. Green, H. H. Michels, and J. C. Browne, J. Chem. Phys. **64**, 3951 (1976).
[10] T. A. Green, H. H. Michels, and J. C. Browne, J. Chem. Phys. **69**, 101 (1978).
[11] T. A. Green, H. H. Michels, J. C. Browne, and M. M. Madsen, J. Chem. Phys. **61**, 5186 (1974).
[12] T. A. Green, J. C. Browne, H. H. Michels, and M. M. Madsen, J. Chem. Phys. **61**, 5198 (1974).
[13] J. Loreau, J. Liévin, P. Palmeri, P. Quinet, and N. Vaeck, J. Phys. B: At. Mol. Opt. Phys. **43**, 065101 (2010).
[14] H.-J. Werner, P. J. Knowles, G. Knizia, F. R. Manby, M. Schütz *et al.*, MOLPRO, version 2006.1 A package of ab initio programs (2006); see http://www.molpro.net.
[15] I. Bouhali, S. Bezzaouia, M. Telmini, and Ch. Jungen, EPJ Web Conf. **84**, 04004 (2015).
[16] M. Telmini and Ch. Jungen, Phys. Rev. A **68**, 062704 (2003).
[17] F. Argoubi, S. Bezzaouia, H. Oueslati, M. Telmini, and Ch. Jungen, Phys. Rev. A **83**, 052504 (2011).
[18] C. H. Greene and B. Yoo, J. Phys. Chem. **99**, 1711 (1995).
[19] C. H. Greene, Phys. Rev. A **28**, 2209 (1983).
[20] Ch. Jungen and F. Texier, J. Phys. B: At. Mol. Opt. Phys. **33**, 2495 (2000).
[21] H. Oueslati, M. Telmini, and Ch. Jungen, Mol. Phys. **104**, 187 (2006).
[22] S. Bezzaouia, M. Telmini, and Ch. Jungen, Phys. Rev. A **70**, 012713 (2004).
[23] H. Oueslati, F. Argoubi, S. Bezzaouia, M. Telmini, and Ch. Jungen, Phys. Rev. A **89**, 032501 (2014).
[24] M. Arif, Ch. Jungen, and A. L. Roche, J. Chem. Phys. **106**, 4102 (1997).
[25] S. Bezzaouia and M. Telmini, *Fundamental and Applied Spectroscopy: Second International Spectroscopy Conference, ISC 2007*, AIP Conf. Proc. No. 935, edited by M. Telmini, N. T. Mliki, and E. Sediki (AIP, Melville, NY, 2007), p. 183.
[26] G. Herzberg, *Molecular Spectra and Molecular Structure, Volume I, Spectra of Diatomic Molecules*, 2nd ed. (Krieger, Malabar, 1989).
[27] T. G. Winter, M. D. Duncan, and N. F. Lane, J. Phys. B: At. Mol. Opt. Phys. **10**, 285 (1977).
[28] J. K. G. Watson, Mol. Phys. **81**, 277 (1994).
[29] M. Aymar, C. H. Greene, and E. Luc-Koenig, Rev. Mod. Phys. **68**, 1015 (1996).
[30] J. Tennyson, Phys. Rep. **491**, 29 (2010).
[31] See Supplemental Material at http://link.aps.org/supplemental/10.1103/PhysRevA.94.022516 for complete Tables of our calculations for all symmetries, as well as for comparisons with the data of Ref. [6].
[32] C. E. Moore, *Atomic Energy Levels*, NSRDS-NBS 467 (National Bureau of Standards, Washington, DC, 1949).
[33] C. H. Greene and Ch. Jungen, Adv. At. Mol. Phys. **21**, 51 (1985).
[34] B. K. Sarpal, J. Tennyson, and L. A. Morgan, J. Phys. B: At. Mol. Opt. Phys. **27**, 5943 (1994).
[35] B. J. Braams, Summary Report of the First Research Coordination Meeting Atomic and Molecular Data for State-Resolved Modelling of Hydrogen and Helium and Their Isotopes in Fusion Plasma, IAEA Nuclear Data Section (Vienna, 2013).